

# GRID CELL MODELING WITH MAPPING REPRESENTATION OF SELF-MOTION FOR PATH INTEGRATION

**Jiru Wang**

College of Computer Science  
Sichuan University  
Chengdu 610065, China  
somnus0722@foxmail.com

**Rui Yan**

College of Computer Science  
Zhejiang University of Technology  
Hangzhou 310023, China  
Ryan@zjut.edu.cn

**Huajin Tang\***

College of Computer Science and Technology  
Zhejiang University  
Hangzhou 310027, China  
htang@zju.edu.cn

## ABSTRACT

The representation of grid cells in the medial entorhinal cortex (MEC) region is crucial for path integration. In this paper, we proposed a grid cell modeling mechanism by mapping the agent's self-motion in Euclidean space to the neuronal activity of grid cells. Our representational model can achieve hexagonal patterns of grid cells from recurrent neural network (RNN) and enables multi-scale path integration for 1D, 2D and 3D spaces. Different from the existing works which need to learn weights of RNN to get the vector representation of grid cells, our method can obtain weights by direct matrix operations. Moreover, compared with the classical models based on continuous attractor network (CAN), our model avoids the connection matrix's symmetry limitation and spatial representation redundancy problems. In this paper, we also discuss the connection pattern between grid cells and place cells to demonstrate grid cells' functioning as a metric for coding space.

## 1 INTRODUCTION

Many species can keep track of their own position without environmental cues and navigate based completely on self-motion information, which is called path integration. The discoveries of spatial sensitive neurons, such as place cells and grid cells, show us spatial cognition may arise from neural activity of these neurons. Exploring how they represent Euclidean space is the key to knowing the brain's representation and encoding for space-related tasks. For unique distributed firing patterns, grid cells have been kept in focus in spatial cognition research field. They are considered as path integrators in brain (Moser et al., 2008; Jacobs et al., 2013; Daniel et al., 2015), helping animals estimate spatial position based on self-motion in the absence of external cues. Grid cells have distributed hexagonal firing patterns covering the environment explored by the animal. A grid cell is characterized by three parameters: spatial scale (the distance between centers of two neighboring firing fields), orientation (the angle between the line joining two neighboring firing fields and a reference axis) and phase (the offset relative to a reference point)(Fyhn et al., 2004; Hafting et al., 2005), as shown in Figure 1.

Many models have been proposed to account for grid cell's hexagonal firing pattern. What they have in common is that the distributed pattern arises from path integration driven by incoming velocity signals from the agent's self-motion in space(Moser et al., 2008). Generally speaking, grid cell can be modeled at the single-cell or network level, depending on whether recurrent interactions between grid cells exist. Oscillatory interference (OI) models are classical single-cell models (Burgess et al., 2010), which have been challenged by further research with other animals except for rats (Yartsev

---

\*Corresponding Author

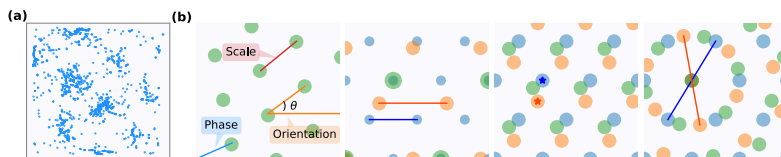


Figure 1: Spatial firing patterns of grid cells. (a) The firing pattern of a specific grid cell from the neuroscience experiment (data from <http://www.ntnu.edu/kavli/research/grid-cell-data>). (b) First column, schematic of grid cell (green circle), being defined by spatial scale, phase and orientation. The next three columns, three grid cells (green, orange and blue circle) with different spatial scales, phases and orientations.

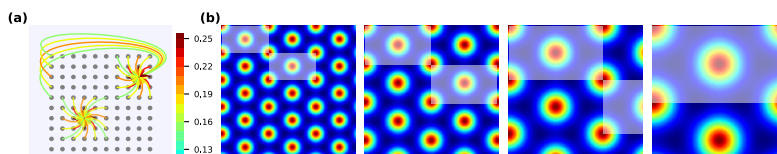


Figure 2: Continuous attractor network (CAN)-based grid cell modeling. (a) Schematic of local, excitatory weighted connections between grid cells. Darker color means stronger connection. (b) Spatial representation redundancy in CAN. Each column illustrates the heat map of all grid cells' activity at the same time in a CAN. For each heat map, taking grid cells covered by a semi-transparent panel as a unit, they will always have the same activity as grid cells in other units.

et al., 2011). The problem of single-cell based models is the relative difference of firing patterns between neighboring cells can hardly be kept across environments where the animal's movement may be very different. CAN-based models are classical network models in which grid cells are connected by short-range excitation and global inhibition (Burak & Fiete, 2009). Activity bumps form spontaneously and move smoothly driven by velocity input and then path integration is done (McNaughton et al., 2006; Fuhs & Touretzky, 2006; Welinder et al., 2010). The problem of CAN-based models is the strong assumption about the wiring between grid cells in the network and they cannot explain the non-topography of spatial phases in the grid cell population. Moreover, many grid cells in CAN share identical firing patterns, which means that their activity level will maintain the same for all time. Here we call it spatial representation redundancy, as shown in Figure 2. For the same spatial area, CANs with smaller spatial scales have more representation redundancy. Recently, researchers try to simulate animals' spatial behaviors through artificial intelligence techniques (Banino et al., 2018; Cueva & Wei, 2018). Specifically, with movement-related velocity signals, a recurrent neural network is trained to perform self-localization in a virtual space and grid-like neuronal representation emerges within the network, similar to grid cells' hexagonal firing patterns observed in rodent's brain. Training-based models show us the potential of using artificial intelligence to test theories about the spatial cognition mechanism in brain. However, they are not preferable because of higher computational cost for training and the slow and unsatisfactory convergence with observed grid-like firing patterns in mammals. In addition, most of the studies on grid cell modeling are done in 2D space. A considerable proportion of animals perform daily activities in 3D space. Therefore a general grid cell modeling mechanism is necessary, at the network level, to achieve grid cell modeling for path integration in spaces of different dimensionality.

In this paper, a novel grid cell modeling mechanism is proposed, in which Jacobian Matrix  $J$ , as the mapping representation, is applied to map the agent's self-motion in Euclidean space to neural activity of grid cells. Based on our proposed modeling mechanism, representational models of grid cells for 1D, 2D and 3D path integration can be achieved and hexagonal firing patterns of grid cells will emerge from recurrent neural networks (RNN). Compared with currently existing models, our representational models will benefit from the following advantages:

1. This modeling mechanism is the combination of single-cell and network based grid cell modeling. Different from IO models, recurrent connections between grid cells are maintained. Compared with CAN-based models, the symmetry limitation on connection matrix and spatial representation redundancy in CAN are effectively avoided in our models.

2. Different from existing training-based RNN models, network weights in our models are derived from the mapping from self-motion in Euclidean space to neuronal activity of grid cells, but not high-cost network training.
3. It is a general mechanism that can achieve representational grid cell models and multi-scale path integration in 1D, 2D and 3D spaces.

In addition, we analyze how grid scale and phase distribution exert influence on our model’s grid coding performance and give referable grid cell modeling instruction. We also underline the necessity of grid cells’ distance metric ability from the engineering modeling perspective and through artificial intelligence technique, we provide an instructive way of thinking about how grid cells function as a metric for coding space.

## 2 THE GENERAL MECHANISM FOR GRID CELL MODELING

When animals move in environment, they can integrate self-motion information through neural representations of Euclidean space in brain. Here a mapping representation is given to map self-motion in Euclidean space to neural activity of grid cells. Jacobian matrix is a very useful tool that has been heavily used in robotic and automation domains to define the dynamic relationship between two different representations in a system. The path integration in brain can be seen as a mapping  $f : \mathbb{R}^m \rightarrow \mathbb{R}^n$  from Euclidean space to grid cells’ activity space and the Jacobian matrix  $\mathbf{J} \in \mathbb{R}^{m \times n}$  can be used for the mapping from  $m$ D space to  $n$ D space. Inspired by this, the mapping from self-motion in Euclidean space to grid cells’ activity is completed based on Jacobian matrix and then a general grid cell modeling mechanism is achieved for path integration in 1D, 2D and 3D space. The flow of the general mechanism for grid cell modeling we proposed is given below:

1. With biologically plausible scales, orientations and phases of grid cells in neuroscience, formulaic description  $s(\mathbf{r}) : \mathbb{R}^m \rightarrow \mathbb{R}^n$  is built to simulate  $n$  grid cells’ firing patterns, a vector function with respect to the  $m$ D Cartesian coordinate  $\mathbf{x}$  in Euclidean space.
2. According to  $s(\mathbf{r})$ , the Jacobian matrix  $\mathbf{J}$  can be obtained to complete the mapping from  $m$ D Euclidean space to  $n$ D vector space of grid cell activity.
3. The grid cell dynamics is achieved based on a recurrent neural network in which recurrent weights can be worked out based on  $\mathbf{J}$  during the mapping process.

For the simple implementation of grid cell modeling in 1D and 2D space, the modeling details are not included and the network weights’ calculation formulas necessary for building the grid cell dynamics will be included in the Appendix. In the following part, we will show how to achieve the mapping representation of grid cells for path integration in 3D space.

## 3 MAPPING REPRESENTATION OF GRID CELLS

In this section, the proposed grid cell modeling mechanism is illustrated by grid cell modeling in 3D space. The specific implementation will be detailed through three parts: the formulaic description of grid cell’s firing pattern, the mapping from self-motion in Euclidean space to neuronal activity of grid cells, and dynamical model for path integration.

### 3.1 FORMULAIC DESCRIPTION OF GRID CELLS’ FIRING PATTERNS

Although a significant corpus of computational models exists in 2D space Guanella et al. (2007); Burak & Fiete (2009); Burgess et al. (2010); Bush & Burgess (2014), models of 3D path integration are comparatively fewer. Grid-like firing patterns in 3D space can be formed by stacking multiple layers of hexagonal firing patterns in the plane and these layers are composed of three repeated layers with specific shift, called face-centered cubic(FCC) lattice. Many modeling studies have predicted the possibility of FCC lattice structure for the grids in the 3D space owing to its higher packing fraction(Federico & Alessandro, 2015; Mathis et al., 2015; Misun & Maguire, 2019). FCC lattice structure is used for modeling 3D grid cells in this paper. Since the actual scale, phase and orientation of 3d grid cell have not been empirically confirmed yet, the biological validity of the chosen scale and phase remains to be verified.

$N$  grid cells are included and the grid cell population's activity is denoted as  $\mathbf{s}(\mathbf{r}) = [s_1, s_2, \dots, s_N]^T$ . The formulaic description of the  $i$ th grid cell's firing patterns can be formed as the function of 3D spatial position  $\mathbf{r}(r_1, r_2, r_3)$ , as shown below:

$$s_i(\mathbf{r}) = \frac{1}{4} \sum_{i=1}^4 \cos(\mathbf{k}_i(\mathbf{r} - \Delta\mathbf{r})) \quad (1)$$

$$\mathbf{K} = \begin{bmatrix} \mathbf{k}_1 \\ \mathbf{k}_2 \\ \mathbf{k}_3 \\ \mathbf{k}_4 \end{bmatrix} = \frac{2\pi}{k_0} \begin{bmatrix} 0 & 0 & \sqrt{3/2} \\ 2/\sqrt{3} & 0 & -1/\sqrt{6} \\ -1/\sqrt{3} & 1 & -1/\sqrt{6} \\ -1/\sqrt{3} & -1 & -1/\sqrt{6} \end{bmatrix}$$

where  $\mathbf{k}_i$  is given as the row vector of the matrix  $\mathbf{K}$ ,  $\Delta\mathbf{r} = (\Delta r_1, \Delta r_2, \Delta r_3)$  and  $k_0$  respectively determine the phase and spatial scale of grid cell firing patterns. Then  $\mathbf{s}(\mathbf{r})$  can be represented as  $\mathbf{s}(\mathbf{r}) = \mathbf{M}\mathbf{g}(\mathbf{r})$ , where

$$\mathbf{M} = \frac{1}{4} \begin{bmatrix} \cos\mathbf{k}_1\Delta\mathbf{r}_1 & \cdots & \cos\mathbf{k}_4\Delta\mathbf{r}_1 & \sin\mathbf{k}_1\Delta\mathbf{r}_1 & \cdots & \sin\mathbf{k}_4\Delta\mathbf{r}_1 \\ \vdots & \vdots & \vdots & \vdots & \vdots & \vdots \\ \cos\mathbf{k}_1\Delta\mathbf{r}_N & \cdots & \cos\mathbf{k}_4\Delta\mathbf{r}_N & \sin\mathbf{k}_1\Delta\mathbf{r}_N & \cdots & \sin\mathbf{k}_4\Delta\mathbf{r}_N \end{bmatrix}$$

$$\mathbf{g}(\mathbf{r}) = [\cos\mathbf{k}_1\mathbf{r} \quad \cdots \quad \cos\mathbf{k}_4\mathbf{r} \quad \sin\mathbf{k}_1\mathbf{r} \quad \cdots \quad \sin\mathbf{k}_4\mathbf{r}]^T$$

Let  $\mathbf{M}^\dagger$  denotes the pseudo-inverse matrix of  $\mathbf{M}$ , then:

$$\mathbf{g}(\mathbf{r}) = \mathbf{M}^\dagger \mathbf{s}(\mathbf{r}) \quad (2)$$

### 3.2 MAPPING FROM EUCLIDEAN SPACE TO NEURAL ACTIVITY

For achieving the mapping from self-motion in Euclidean space to grid cell population activity, Jacobian matrix is expected to be used as the mapping representation, which is a matrix of all first-order partial derivatives of the vector-valued function  $\mathbf{s}$ . With  $\mathbf{s}(\mathbf{r}): \mathbb{R}^3 \rightarrow \mathbb{R}^N$  and the corresponding Jacobian matrix  $\mathbf{J} \in \mathbb{R}^{3 \times N}$ , the following formula is obtained:

$$\frac{d\mathbf{s}}{dt} = \mathbf{J} * \frac{d\mathbf{r}}{dt} = \mathbf{J} * \mathbf{v}_t \quad (3)$$

$$\mathbf{J} = \begin{bmatrix} \partial s_1 / \partial r_1 & \partial s_1 / \partial r_2 & \partial s_1 / \partial r_3 \\ \vdots & \vdots & \vdots \\ \partial s_N / \partial r_1 & \partial s_N / \partial r_2 & \partial s_N / \partial r_3 \end{bmatrix}$$

and  $\mathbf{v}_t = [v_1^t, v_2^t, v_3^t]^T$  is the velocity vector in Euclidean space at time  $t$ . Combining with  $\mathbf{s}(\mathbf{r})$  in Eq. 1,  $\mathbf{J}$  can be worked out:

$$\mathbf{J} = \begin{bmatrix} \frac{\partial \mathbf{s}}{\partial x} & \frac{\partial \mathbf{s}}{\partial y} & \frac{\partial \mathbf{s}}{\partial z} \end{bmatrix} = [\mathbf{M}\mathbf{B}_1\mathbf{g}(\mathbf{r}) \quad \mathbf{M}\mathbf{B}_2\mathbf{g}(\mathbf{r}) \quad \mathbf{M}\mathbf{B}_3\mathbf{g}(\mathbf{r})] \quad (4)$$

$$\mathbf{B}_m = \begin{bmatrix} \mathbf{0} & \mathbf{B}_{m1} \\ \mathbf{B}_{m2} & \mathbf{0} \end{bmatrix}$$

$$\mathbf{B}_{m1} = \text{diag}[-K_{1m}, -K_{2m}, -K_{3m}, -K_{4m}] \quad \mathbf{B}_{m2} = \text{diag}[K_{1m}, K_{2m}, K_{3m}, K_{4m}]$$

Combined with Eq. 2 and 4, Eq. 3 can be translated and finally the following formula can be obtained:  $d\mathbf{s}/dt = \sum_{i=1}^3 \mathbf{W}^i * v_i^t * \mathbf{s}$  and  $\mathbf{W} = [\mathbf{M}\mathbf{B}_1\mathbf{M}^\dagger \quad \mathbf{M}\mathbf{B}_2\mathbf{M}^\dagger \quad \mathbf{M}\mathbf{B}_3\mathbf{M}^\dagger]$

### 3.3 GRID CELL DYNAMICS FOR PATH INTEGRATION

The mapping representation, Jacobian matrix, has been introduced for mapping self-motion in Euclidean space to neural activity of grid cells. To organize grid cells through recurrent connections and complete path integration, the rate-based dynamics of grid cells can be formulated as  $\tau d\mathbf{s}/dt = f(\sum_{i=1}^3 \mathbf{W}^i * v_i^t * \mathbf{s})$  and the activation function  $f(x) = 0$  if  $x \leq 0$  else  $f(x) = 1$ .

## 4 EXPERIMENT RESULTS

In this section, grid cell modeling is done based on the modeling mechanism we proposed for multi-scale path integration in 2D and 3D spaces. In our model, grid cells are grouped into five modules. Grid cells in each module are organized into a recurrent neural network (called sub-RNN below) for multi-scale path integration and they have the same spatial scale and orientation but different phases.

### 4.1 GRID FIRING PATTERNS

Two grid cell models are firstly completed respectively in 2D and 3D space, which have similar network structures. Both of them include 5 sub-RNNs with different grid scales for path integration and each network includes a grid cell population with different phases but the same scale.

In 2D space, Figure 3(a) shows the agents' random exploration in a  $25m^2$  square area. Five grid cells are randomly selected respectively from sub-RNNs with different grid scales and their spatial activity maps are illustrated in Figure 3(b). In the same way, we also obtain spatial firing patterns of five grid cells randomly selected from the 3D grid cell model, as shown in Figure 4 (a).

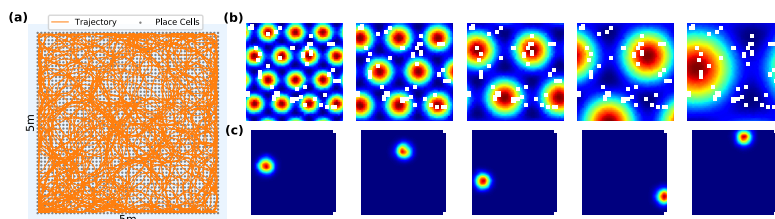


Figure 3: Exploration of the agent in 2D space. (a) The agent's random exploration in a  $25m^2$  area (orange line) and place cells (grey circles) uniformly covering the whole area. (b) Multi-scale spatial activity maps of grid cells. (c) Spatial activity maps of place cells.

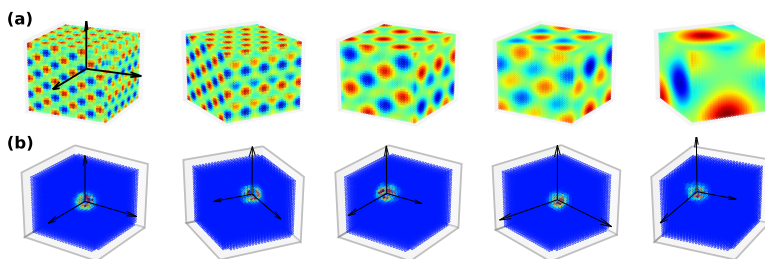


Figure 4: Grid firing patterns in 3D space. (a) Multi-scale spatial activity maps of grid cells. (b) Spatial activity maps of place cells.

### 4.2 GRID CODING PERFORMANCE ANALYSIS

The grid cell models' coding performance has relationship with grid cells' spatial scale and phase distribution. In the following experiments, statistical analysis based on different network size are done both in 2D and 3D space to arrive at more general conclusions and derive some helpful modeling instructions. An indicator AGE quantifying the models' coding performance is defined:  $AGE = (1/N) \sum_{t=0}^T \|Gp^t - Gg^t\|$ , which is all grid cells' average of accumulated grid coding error during exploration.  $N$  is the number of grid cells involved,  $Gp^t = (Gp_1^t, Gp_2^t, \dots, Gp_N^t)$  and  $Gg^t = (Gg_1^t, Gg_2^t, \dots, Gg_N^t)$  respectively represent the population activity of grid cells derived from our models and the corresponding ground truth activity.  $Gp_i^t$  is the  $i$ th grid cell's activity at time  $t$ .

#### 4.2.1 GRID SCALE

Grid cells with different spatial scales have varying sensitivity to velocity input, so the grid coding performance of sub-RNNs with different scales will differ from each other. Signals from the

same exploration trajectory (Figure 5 (b)) are taken as network input for analyzing the relationship between grid scale and coding performance. The phase distribution of grid cells generated by hexagonal tiling method is set for all sub-RNNs, as shown in Figure 5 (a).

The activity of five grid cells from sub-RNNs with different spatial scales in our model is recorded and compared with the ground truth activation (Figure 5 (d)). It can be seen that sub-RNNs with smaller scales are more sensitive to the external input and networks with larger scales are easier to keep stable grid coding performance. The statistical result of AGE for the five sub-RNNs in Figure 5 (c) and the experiment result in 2D space in Figure 10 (in Appendix) also demonstrate this point.

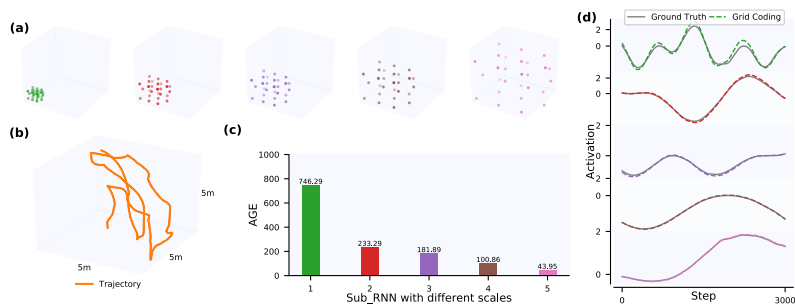


Figure 5: Grid coding performance analysis based on different grid scales in 3D space. (a) The phase distribution of sub-RNNs with different scales. (b) The agent’s exploring trajectory in a  $125m^3$  area. (c) Histogram showing accumulated coding error of each sub-RNN after path integration following the simulation trajectory in (b). (d) The comparison between the coding result derived from our model and the ground truth activity of the selected grid cells in (a).

#### 4.2.2 GRID PHASE

In experiment, phases of grid cells are respectively generated through random uniform distribution, square tiling and hexagonal tiling, as shown in Figure 6 (a) and Figure 11 (a) (in Appendix). For the same grid cell model with the same moving trajectory as input signals, we record its grid coding performance in the cases of the different phase distributions, as shown in Figure 6 (b) and Figure 11 (b) (in Appendix). Furthermore, to ensure valid conclusive analysis, grid cell models with different network sizes are tested. As illustrated in Figure 6 (c), the vertical axis represents models’ AGE while the horizontal axis represents the sub-RNN’s size in models. For example, ‘27’ means each sub-RNN includes 27 grid cells and the whole model includes  $27 \times 5$  grid cells.

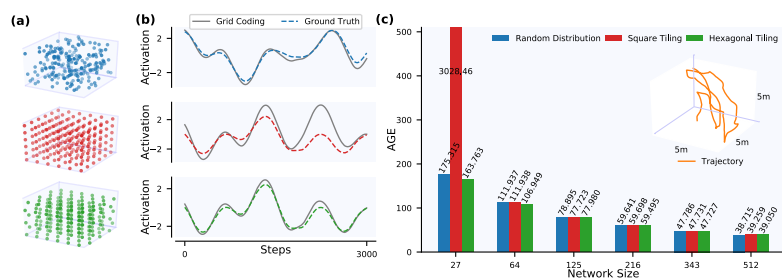


Figure 6: Grid coding performance analysis based on different phase distributions in 3D space. (a) The phase distributions respectively generated by uniform random distribution, square tiling and hexagonal tiling. (b) The comparison between the ground truth and grid coding derived from our model for three grid cells randomly selected in the cases of different phase distribution. (c) Histogram showing, with different network sizes, accumulated grid coding error of the whole model in the case of different phase distributions.

Statistical results in 3D and 2D space (in Appendix) show that with smaller network size and fewer grid cells, the above three phase distributions vary greatly, leading to different coding performance. With the network size gradually increases, the phase distributions gradually tend to be uniform coverage, leading to similar coding performance. To be specific, the square tiling can make better

coding performance only when the network size is larger, unsuitable for smaller networks while the hexagonal tiling can bring the best coding performance when the network size is smaller. Moreover, unless the uniform random distribution can make better coding performance in all cases, we won't choose it even it can bring the best coding performance in some cases. This is because principally it is an unstable method relying heavily on random seed we choose. In brief, the hexagonal tiling is a better phase generation method for grid cell modeling, which is more suitable for different network sizes and can yield better coding performance in most cases.

### 4.3 PATH INTEGRATION

There is evidence that in mammals, place representation exists in close anatomical proximity to grid cell (Barry & Burgess, 2014). Grid cells in adult rodents appear to contribute to the neural activity of place cells (Zhang et al., 2013; de Almeida et al., 2009). We first build two grid cell models in 2D and 3D space, respectively including five sub-RNNs for multi-scale path integration. Velocity signals from simulated trajectories are provided as network input. Sub-RNNs are projected to place cells via a linear layer for path prediction. The vector of activities in the place cells corresponding to the current position was provided as a supervised training signal at each time step.

Figure 7 and Figure 8 show us the path prediction results in a  $25m^2$  2D space and a  $125m^3$  3D space. To keep localization error lower than 0.25m, 625 and 8000 place cells are set for spatial location decoding. In the grid cell models, each sub-RNN includes 216 grid cells.

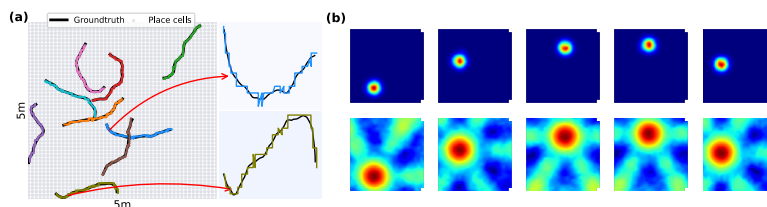


Figure 7: Path integration in 2D space. (a) A  $25m^2$  area with place cells uniformly covered during the experiment. Self-location decoded from our model (varying colors) resembles the actual path (black). (b) Top, firing fields of five place cells. Bottom, the corresponding predictive results from our model.

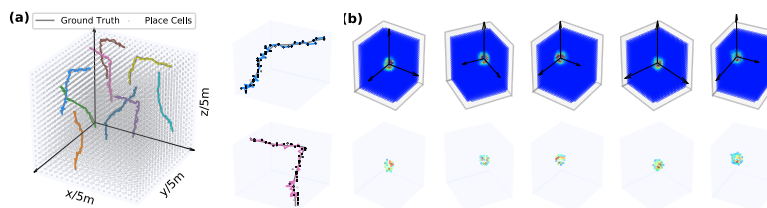


Figure 8: Path planning of grid cells in 3D space. (a), (b) Similar to Figure 7

As shown in Figure 7 (a), with 625 place cells uniformly covering the working area, 9 trajectories are simulated. the black lines represent the ground truth and colored lines demonstrate the predicted results. Figure 7 (b) illustrates the ground truth activity of five place cells and the decoding results from our model. The spatial locations and the corresponding place cells can be rightly predicted.

### 4.4 FUNCTIONING AS A METRIC FOR CODING SPACE

According to the neuroscience definition of place cell, one place cell will be only activated in one specific spatial location in an area and then represents one specific location in the area. So when it comes to engineering modeling, it means that there are enough place cells that can cover the agent's whole working area and ensured the spatial coding accuracy is kept at an acceptable level. As shown in Figure 9 (a), for a  $5 \times 5m^2$  2D area, 625 place cells are needed to uniformly cover the whole area and keep the localization error within an acceptable range (here 0.2m) and for a  $20 \times 20m^2$  2D area,

1600 place cells are needed. However, when it comes to 3D space, 15625 and 64000 place cells are respectively are needed. The huge increase in the number of place cells compared with 2D space, adding more computational burden to the system.

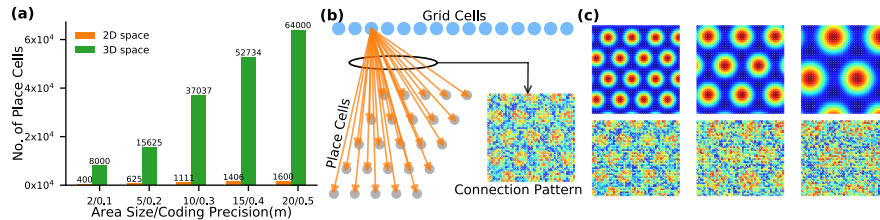


Figure 9: Analysis about grid cells’ metric ability. (a) Histogram showing the numbers of place cells needed for spatial representation in 2D and 3D spaces. (b) Schematic of the connection pattern between grid cells and place cells. (c) Top, the spatial activity maps of five grid cells with different spatial scales in our 2D grid cell model. Bottom, the connection pattern between the five grid cells to all place cells.

Neuroscience shows us that grid cells are organized in distinct modules, where each module contains grid cells with similar scale and orientation of the firing pattern (Stensola et al., 2012; Gu et al., 2018). The joint spatial response of grid cells in only several modules is enough to generate an enormous diversity of ensemble activity because of the varying spatial scales and phases of grid cells. It is similar to the combination theory (Fiete et al., 2008; Moser et al., 2015). Take the combination lock as an example, more than tens of thousands of unique password series can be generated by the combination of only several modules of decimal digits. The coding advantage of grid cells should be fully exerted in spatial cognition. In Banino et al. (2018), a recurrent network was trained to perform path integration, leading to the emergence of representations resembling grid cells, furnishing agents with a Euclidean spatial metric. No details have yet been given about how grid cell functions as a metric. Here we go a step further about the connection pattern between grid cells and place cells, and do some preliminary exploration of grid cells’ functioning as a metric for coding space.

According to Figure 9 (b), connection patterns between grid cells and place cells are mapped as heat maps, as shown in the bottom of Figure 9 (c), which exhibit spatially tuned grid-like patterns resembling grid cells. The implication of this discovery is instructive: though there is no clear conclusion about the connection between grid and place cells in neuroscience, the weight training between grid cells and place cells to furnish the agent with the ability to decode self-locations leads to grid-like connection patterns. We should ponder it from another perspective: connection weights can be seen as grid cells’ contributions during spatial location decoding, which, to some extent, is spatially tuned and strongly correlated with its own firing patterns. If the delicate relationship between them can be determined, grid cells can really function as a direct metric for coding space and do distance measure, path planning and navigation without place cells. The exploration of the grid-like connection pattern provides a referable and instructive way of thinking about grid cells’ functioning as the metric of coding space.

## 5 CONCLUSION

In this paper, a general grid cell modeling mechanism is given for mapping the self-motion in Euclidean space to grid cell’s neural activity, achieving path integration in 1D, 2D and 3D space. Path integration is done at the network level and recurrent connections between grid cells are maintained. Different from training-based models, network weights can be worked out during the mapping process. Compared with classical CAN-based models, there is no symmetry limitation on the connection matrix and spatial representation redundancy. We go a step further based on the grid cell built following our proposed modeling mechanism. The effect of grid scale and phase on our models’ grid coding performance is analyzed for deriving helpful grid cell modeling instructions to achieve accurate path integration in space of different dimensionality. In addition, the necessity of grid cells’ function as a metric for coding space is underlined from the engineering modeling perspective and an instructive and new way of thinking about exploring the distance metric mechanism of grid cells, which is the import research topic we will look further into.

## ACKNOWLEDGMENTS

This work was supported by the National Natural Science Foundation of China under Grant No. 61773271 and 61673283.

## REFERENCES

- Andrea Banino, Caswell Barry, Benigno Uribe, Charles Blundell, Timothy Lillicrap, Piotr Mirowski, Alexander Pritzel, and et. al. Vector-based navigation using grid-like representations in artificial agents. *Nature*, 557(7705):429–433, 2018.
- Caswell Barry and Neil Burgess. Neural mechanisms of self-location. *Current Biology*, 24(8):R330–339, 2014.
- Yoram Burak and Ila R. Fiete. Accurate path integration in continuous attractor network models of grid cells. *PLOS Computational Biology*, 5(2):1–16, 2009.
- Neil Burgess, Caswell Barry, and John O’Keefe. An oscillatory interference model of grid cell firing. *Hippocampus*, 17(9):801–812, 2010.
- Daniel Bush and Neil Burgess. A hybrid oscillatory interference/continuous attractor network model of grid cell firing. *The Journal of neuroscience : the official journal of the Society for Neuroscience*, 34(14):5065–5079, 2014.
- Christopher J. Cueva and Xue-Xin Wei. Emergence of grid-like representations by training recurrent neural networks to perform spatial localization. In *International Conference on Learning Representations*, 2018. URL <https://openreview.net/forum?id=B17JTOe0->.
- Bush Daniel, Barry Caswell, Manson Daniel, and Burgess Neil. Using grid cells for navigation. *Neuron*, 87(3):507–520, 2015.
- Licurgo de Almeida, Marco Idiart, and John E. Lisman. The input-output transformation of the hippocampal granule cells: from grid cells to place fields. *The Journal of neuroscience*, 29(23):7504–7512, 2009.
- Stella Federico and Treves Alessandro. The self-organization of grid cells in 3d. *eLife*, 4, 2015.
- Ila R. Fiete, Yoram Burak, and Ted Brookings. What grid cells convey about rat location. *Journal of Neuroscience*, 28(27):6858–6871, 2008.
- Mark C. Fuhs and David S. Touretzky. A spin glass model of path integration in rat medial entorhinal cortex. *Journal of Neuroscience*, 26(16):4266–4276, 2006.
- Marianne Fyhn, Sturla Molden, Menno P. Witter, Edvard I. Moser, and May-Britt Moser. Spatial representation in the entorhinal cortex. *Science*, 305(5688):1258–1264, 2004.
- Yi Gu, Sam Lewallen, Amina A. Kinkhabwala, Cristina Domnisoru, Kijung Yoon, Jeffrey L. Gauthier, Ila R. Fiete, and David W. Tank. A map-like micro-organization of grid cells in the medial entorhinal cortex. *Cell*, 175(3):736–750.e30, 2018.
- Alexis Guanella, Kiper Daniel, and Paul Verschure. A model of grid cells based on a twisted torus topology. *International Journal of Neural Systems*, 17(04):231–240, 2007.
- Torkel Hafting, Marianne Fyhn, Sturla Molden, May-Britt Moser, and Edvard I. Moser. Microstructure of a spatial map in the entorhinal cortex. *Nature*, 436:801–806, 2005.
- Joshua Jacobs, Christoph T. Weidemann, Jonathan F. Miller, Alec Solway, and et al. Direct recordings of grid-like neuronal activity in human spatial navigation. *Nature neuroscience*, 16(9):1188, 2013.
- Alexander Mathis, Martin B. Stemmler, and Andreas VM. Herz. Probable nature of higher-dimensional symmetries underlying mammalian grid-cell activity patterns. *eLife*, 4:e05979, 2015.

- Bruce L. McNaughton, Francesco P. Battaglia, Ole Jensen, Edvard I. Moser, and May-Britt Moser. Path integration and the neural basis of the 'cognitive map'. *Nature Reviews Neuroscience*, 7: 663–678, 2006.
- Kim Misun and Eleanor A. Maguire. Can we study 3d grid codes non-invasively in the human brain? methodological considerations and fmri findings. *NeuroImage*, 186:667–678, 2019.
- Edvard I. Moser, Emilio Kropff, and May-Britt Moser. Place cells, grid cells, and the brain’s spatial representation system. *Annual review of neuroscience*, 31:69–89, 2008.
- May Britt Moser, David C. Rowland, and Edvard I. Moser. Place cells, grid cells, and memory. *Cold Spring Harbor Perspectives in Biology*, 7(2):a021808, 2015.
- Hanne Stensola, Tor Stensola, Trygve Solstad, Kristian Fraland, May-Britt Moser, and Edvard I. Moser. The entorhinal grid map is discretized. *Nature*, 492(7427):72–78, 2012.
- Peter E. Welinder, Yoram Burak, and Ila R. Fiete. Grid cells: The position code, neural network models of activity, and the problem of learning. *Hippocampus*, 18(12):1283–1300, 2010.
- Michael M. Yartsev, Menno P. Witter, and Nachum Ulanovsky. Grid cells without theta oscillations in the entorhinal cortex of bats. *Nature*, 479:103–107, 2011.
- Sheng-Jia Zhang, Jing Ye, Chenglin Miao, Albert Tsao, Ignas Cerniauskas, Debora Ledergerber, May-Britt Moser, and Edvard I. Moser. Optogenetic dissection of entorhinal-hippocampal functional connectivity. *Science*, 340(6128), 2013.

## A APPENDIX

### A.1 GRID CELL MODELING IN 1D SPACE

The position in 1D space is denoted as  $r$ , which is a scalar value. There are  $N$  grid cells in the neural network and  $\mathbf{s}(r) = [s_1(r), s_2(r), \dots, s_N(r)]^T$  (or  $\mathbf{s} = [s_1, s_2, \dots, s_N]^T$ ) represents the grid cell population activity. The formulaic description of grid cell firing patterns we used as below:

$$s_i(r) = \frac{1}{2} \cos(k_0(r - \Delta r)) + \frac{1}{2}$$

where  $\Delta r$  and  $k_0$  respectively determine the grid pattern phase and spatial scale. The weight can be calculated as follows:

$$\mathbf{W} = \mathbf{M} * \mathbf{K}_0 * \mathbf{M}^\dagger$$

where

$$\mathbf{K}_0 = \begin{bmatrix} 0 & -k_0 \\ k_0 & 0 \end{bmatrix}$$

$$\mathbf{M} = \begin{bmatrix} \cos k_0 \Delta r_1 & \sin k_0 \Delta r_1 \\ \vdots & \vdots \\ \cos k_0 \Delta r_N & \sin k_0 \Delta r_N \end{bmatrix}$$

$\mathbf{M}^\dagger$  denotes the pseudo-inverse matrix of  $\mathbf{M}$  and can be obtained through the singular value decomposition of matrix  $\mathbf{M}$ . Finally, the dynamics of grid cells in 1D space is  $\tau ds/dt = f(\mathbf{W} * v_t * \mathbf{s})$  where  $f(x) = 0$  if  $x \leq 0$  else  $f(x) = 1$  and  $v_t$  is the moving velocity in 1D space.

### A.2 GRID CELL MODELING IN 2D SPACE

The position in 2D space is denoted as  $\mathbf{r}=(x, y)$ . There are  $N$  grid cells in the neural network and  $\mathbf{s}(\mathbf{r}) = [s_1(\mathbf{r}), s_2(\mathbf{r}), \dots, s_N(\mathbf{r})]^T$  (or  $\mathbf{s} = [s_1, s_2, \dots, s_N]^T$ ) represents the grid cell population activity. The formulaic description of grid cell firing patterns we used as below:

$$s_i(\mathbf{r}) = \frac{1}{3} \sum_{j=1}^3 \cos(\mathbf{k}_j(\mathbf{r} - \Delta \mathbf{r})) + \frac{1}{3}$$

where  $s_i(\mathbf{r})$  is the  $i$ th grid cell's activity.  $\Delta\mathbf{r}=(\Delta x, \Delta y)$  determine the grid pattern phase.  $\mathbf{k}_j$  can be given as the row vector of the matrix  $\mathbf{K}$ :

$$\mathbf{K} = \begin{bmatrix} \mathbf{k}_1 \\ \mathbf{k}_2 \\ \mathbf{k}_3 \end{bmatrix} = k_0 \begin{bmatrix} \cos(\frac{\pi}{6} - \theta) & \sin(\frac{\pi}{6} - \theta) \\ \cos(-\frac{\pi}{6} - \theta) & \sin(-\frac{\pi}{6} - \theta) \\ \cos(-\frac{\pi}{2} - \theta) & \sin(-\frac{\pi}{2} - \theta) \end{bmatrix}$$

where  $k_0 = 2\pi/T$ .  $T$  and  $\theta$  respectively represent the grid scale and direction, which are same for grid cells in a neural network. The weight can be calculated as follows:

$$\mathbf{W}^m = \mathbf{M} * \mathbf{B}_m * \mathbf{M}^\dagger \quad (m = 1, 2)$$

where

$$\mathbf{B}_m = \begin{bmatrix} \mathbf{0} & \mathbf{B}_{m1} \\ \mathbf{B}_{m2} & \mathbf{0} \end{bmatrix}$$

$$\mathbf{B}_{m1} = \text{diag}([-K_{1m}, -K_{2m}, -K_{3m}]) \quad \mathbf{B}_{m2} = \text{diag}([K_{1m}, K_{2m}, K_{3m}])$$

$$\mathbf{M} = \frac{1}{3} \begin{bmatrix} \cos k_1 \Delta \mathbf{r}_1 & \cos k_2 \Delta \mathbf{r}_1 & \cos k_3 \Delta \mathbf{r}_1 & \sin k_1 \Delta \mathbf{r}_1 & \sin k_2 \Delta \mathbf{r}_1 & \sin k_3 \Delta \mathbf{r}_1 \\ \vdots & \vdots & \vdots & \vdots & \vdots & \vdots \\ \cos k_1 \Delta \mathbf{r}_N & \cos k_2 \Delta \mathbf{r}_N & \cos k_3 \Delta \mathbf{r}_N & \sin k_1 \Delta \mathbf{r}_N & \sin k_2 \Delta \mathbf{r}_N & \sin k_3 \Delta \mathbf{r}_N \end{bmatrix}$$

It should be noted that  $\mathbf{M}^\dagger$  denotes the pseudo-inverse matrix of  $\mathbf{M}$  and can be obtained through the singular value decomposition of matrix  $\mathbf{M}$ . Finally, the dynamics of grid cells in 2D space is  $\tau ds/dt = f(\sum_{i=1}^2 \mathbf{W}^m * v_m^t * s)$  where  $f(x) = 0$  if  $x \leq 0$ , else  $f(x) = 0$  and  $\mathbf{v}_t = [v_1^t, v_2^t]^T$  is the moving velocity vector in 2D space.

### A.3 GRID CODING PERFORMANCE ANALYSIS IN 2D SPACE

Grid coding performance analysis based on different grid scales in 2D space:

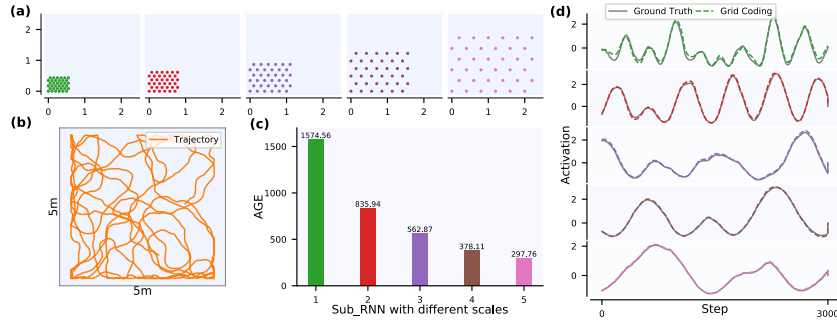


Figure 10: Grid coding performance analysis based on different grid scales in 2D space. (a) The phase distribution of sub-RNNs with different scales. (b) The agent's exploring trajectory in a  $25m^2$  area. (c) Histogram showing accumulated coding error of each sub-RNN after path integration following the simulation trajectory in (b). (d) The comparison between the coding result derived from our model and the ground truth activity of the selected grid cells in (a).

Grid coding performance analysis based on different phase distributions in 2D space:

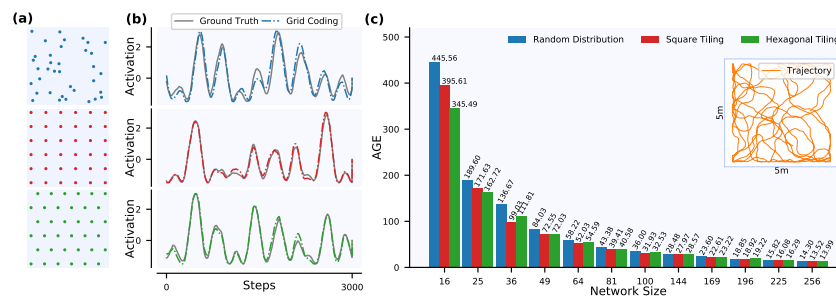


Figure 11: Grid coding performance analysis based on different phase distributions in 2D space. (a) The phase distributions respectively generated by uniform random distribution, square tiling and hexagonal tiling. (b) The comparison between the ground truth and grid coding derived from our model for three grid cells randomly selected in the cases of different phase distribution. (c) Histogram showing, with different network sizes, accumulated grid coding error of the whole model in the case of different phase distributions.